USING ELETRODYNAMIC TETHERS TO PERFORM STATION-KEEPING MANEUVERS IN LEO SATELLITES

Thais Carneiro Oliveira[(1)], **and Antonio Fernando Bertachini de Almeida Prado**[(2)]
[(1)(2)] *National Institute for Space Research (INPE), Av. dos Astronautas 1758 São José dos Campos – SP – Brazil ZIP code 12227-010,+55 12 32086000, thais.tata@gmail.com and antonio.prado@inpe.br*

Abstract: *This paper analyses the concept of using an electrodynamic tether to provide propulsion to a space system with an electric power supply and no fuel consumption. The present work is focused on orbit maintenance and on re-boost maneuvers for tethered satellite systems. The analyses of the results will be performed with the help of a practical tool called "Perturbation Integrals" and an orbit integrator that can include many external perturbations, like atmospheric drag, solar radiation pressure and luni-solar perturbation.*

Keywords: *Electromagnetic Tether, Station-Keeping Maneuver, Orbital Maneuver, Tether Systems, Disturbing Forces.*

1. Introduction

Space tether is a promising and innovating field of study, and many articles, technical reports, books and even missions have used this concept through the recent decades. An overview of the space tethered flight tests missions includes the Gemini tether experiments, the OEDIPUS flights, the TSS-1 experiments, the SEDS flights, the PMG, TiPs, ATEx missions, etc [1-6].

This paper analyses the potential of using an electrodynamic tether to provide propulsion to a space system with an electric power supply and no fuel consumption. The present work is focused on orbit maintenance and re-boosts maneuvers for tethered satellite systems (TSS). This type of system consists of two or more satellites orbiting around a planet linked by a cable or a tether [7]. A conductive tether with electrons passing through a magnetic field generates electromagnetic propulsion due to the induced Lorentz force. The direction of this electromagnetic force depends on the directions of the magnetic field and the current flow.

The control of the magnitude of the induced Lorentz force can be easily achieved with a variable resistance through the tether. One of the most known proposed tethered missions that include a battery to re-boost the orbit is devoted to the International Space Station (ISS) [8,9,10].

Low-orbits with drag-free considerations is studied in many articles and it has already reached the level of real missions, with the goal of extending the life-time of the satellite using fuel-consumption methods in order to overcome the atmospheric drag [12,13,14,15]. The drag-free orbits are essential to missions that must have a low orbit and no drift in the orbit.

The analyses of the results is performed with the help of a practical tool called "Perturbation Integrals" and an orbit integrator that can include many external perturbations, like atmospheric drag, solar radiation pressure and third body perturbation of the Sun and the Moon [16,17].

2. Mathematical Models

This section describes the mathematical models used in the present paper.

2.1. The Electromagnetic Tether

The idea of the paper is to create an electromagnetic propulsion in the opposite direction of the disturbing forces. It is considered two main situations for the station-keeping maneuvers. One of them includes the reduction of the magnitude of all the disturbing forces considered in the model and the other one includes only the reduction of the atmospheric drag.

The mathematical formulation of the induced Lorentz force on an electromagnetic tether, whether it is used for thrust or drag, is given as follows [6,7,8,9,10,11].

$$\boldsymbol{F}_{mag} = \int_0^L I d\boldsymbol{L}\, x\boldsymbol{B} \tag{1}$$

where $\boldsymbol{F}_{mag}$ is the force exerted on the tether by the magnetic field [N]; I is the tether current [A]; $d\boldsymbol{L}$ is the differential element of the tether length and it points in the direction of a positive current flow [m]; $\boldsymbol{B}$ is the magnetic field [T] and L is the tether length [m]. In Eq. (1), it is assumed that the current I is not uniform across the system. The non-uniformity is due to the bare tether system that is considered in this work and later explained.

The magnetic field model used in this paper is the International Geomagnetic Reference Field (IGRF-12) and it is well explained in the literature [18,19,20,21].

The electrodynamic bare tether is proposed in this paper. The bare tether is a breakthrough that allows the tether to capture more electrons and exempt an anode as the tether itself collects the electrons [6,8].

The tether itself requires a power supply to overcome the induced EMF and it must be linked to m_1. The battery is understood as the load resistance. There is a need also to have an electron emitter m_1. The end masses of the tether are considered to be rectangular shaped. The side of each end mass is the same and its area is given by a_1 for the end mass m_1 and a_2 for m_2. In mathematical terms, the electron collection in bare tethers, when the bias is positive, is given as follows [9][22].

$$I(l) = \frac{2}{3} K_2 n_e r_t \sqrt{E_0} [l_c^{\frac{3}{2}} - \left(l - \frac{I_{max} R_{load}}{E_0}\right)^{3/2}] \tag{2}$$

where $K_2 = 1.9x10^{-13} C^{1.5}/kg^{0.5}$, n_e denotes the ionospheric electron density, r_t is the tether radius, E_0 is the motional electric field [V/m], l_c is the electron collection length, I_{max} is the maximum value of the current and it does not change after the voltage bias becomes negative and R_{load} is the impedance load [6]. The R_{load} can be understood in this context as the battery that is used to drive the current against the induced EMF. The induced EMF £ is given as follows [3].

$$£ = \int_0^L (\boldsymbol{V}_r x \boldsymbol{B}) \cdot d\boldsymbol{L} \tag{3}$$

where $\boldsymbol{V}_r$ is the velocity of the spacecraft relative to the magnetic field and $\boldsymbol{B}$ is the magnetic field. It is assumed that the magnetic field rotates at the same rate of the Earth. The tether electron collection length l_c is given by Eq. (5) [6].

$$l_c = l_{tot} - \frac{I_{max} R_{load}}{E_0} \tag{4}$$

For the interval where the voltage bias is negative, the maximum current is given by [6] Eq. (6).

$$I_{max} = \frac{2}{3} K_2 n_e r_t \sqrt{E_0} l_c^{\frac{3}{2}} \tag{5}$$

The bias voltage V* can be written as shown in Eq. (7) [9].

$$V^* = E_0 l - I_{max} R_{load} \tag{6}$$

The first term on the right side of Eq. (7) can be understood as the induced EMF and the second is the rise voltage that the battery must apply in order to guarantee that the current flows in the opposite direction.

2.2. The Disturbing Forces

The disturbing forces included in this work are: atmospheric drag, solar radiation pressure and third-body perturbations from the Sun and the Moon.

The magnitude of the atmospheric drag is proportional to the product of the atmospheric density ρ, and the square of the relative velocity, $\dot{r}'^2$. The relative velocity is actually the velocity of the spacecraft with respect to the velocity of the atmosphere. The acceleration of the atmospheric drag, $\boldsymbol{a}_{drag}$, is given as follows [23].

$$\boldsymbol{a}_{drag} = -\frac{1}{2} \rho \frac{C_D A_D}{m} \dot{r}' \dot{\boldsymbol{r}}' \tag{7}$$

where C_D is the drag coefficient, m is the mass of the spacecraft, A_D is the area of the cross-sectional area facing the flow.

The model of the atmosphere for the density ρ that was implemented in this paper is a hybrid standard atmosphere model that follows the 1976 U.S. Standard Atmosphere [24] for the altitude from 0 up to 86 km and the 1962 U.S. Standard Atmosphere [25] that models all the layers from 86 to 2000 km of altitude.

The mathematical formulation for the acceleration due to a third-body $\boldsymbol{a}_{third-body}$ is given by Eq. (9) [23].

$$\boldsymbol{a}_{third-body} = G m_t \left(\frac{1}{r_{st}^3} \boldsymbol{r}_{st} - \frac{1}{r_{et}^3} \boldsymbol{r}_{et} \right) \tag{8}$$

where m_t is the mass of the third-body, G is the gravitational constant, $\boldsymbol{r}_{st}$ is the vector from the spacecraft to the centre of mass of the third-body and $\boldsymbol{r}_{et}$ is the vector from the centre of mass of the Earth to the centre of mass of the third-body.

The solar radiation pressure perturbation occurs when a light beam collides with the surface of the spacecraft. If the solar radiation centre of pressure acts on the centre of mass of the spacecraft, then the change of the energy results in an orbital modification. This situation is assumed in the present paper. The acceleration due to the solar radiation pressure $\boldsymbol{a}_{radiation}$ is given as follows [26,27].

$$\boldsymbol{a}_{radiation} = \gamma \frac{\bar{h}_0(1+\varepsilon)}{c} \frac{r_{ES}^2}{R_S^2} \frac{S}{m} cos^2\beta \tag{9}$$

where γ defines the shadow region, S is the area of the surface illuminated by the Sun, $\bar{h}_0$ is the solar radiation power ($\approx 1360\ W/m^2$), ε is the reflectivity coefficient that depends on the type of the material of the surface that varies from zero (absorbers everything) to one (reflects everything), r_{ES} is the mean distance from the Earth to the Sun, R_S is the distance from the centre of gravity of the spacecraft to the Sun and β describes the angle of the incident light over the surface of the satellite.

2.3. The Perturbation Integrals

The integral approach obtains the integral for one orbital period of the magnitude of the disturbing forces. It is given as follows [16].

$$\text{inte} = \int_0^{\text{T}} |\mathbf{F}| \text{dt} \tag{10}$$

where **F** is the disturbing force per unit mass [m/(s^2·kg)] and T is the period of the orbit.

3. Results

The coordinate system presented in the results is a non-inertial one that defines the attitude of the tether. The X-axis is parallel to the position vector of the centre of the mass of the system from the centre of the Earth. The origin O is the centre of the mass of the system. The Z-axis points towards the direction of the angular momentum of the orbit and the Y-axis completes the right-handed set of the coordinate system. The Pitch angle α is the angle between the projection of the second end mass of the system m_2 on the X-Y plane and the X axis. The Roll angle γ is the angle between the position of the vector m_2 and its projection on the X-Y plane.

3.1. The Initial Parameters

A number of simulations are carried out to analyze the effects of the electromagnetic tether control. The initial parameters may change for each simulation. The new initial parameters

are given, if there is a modification of the parameters given in Tables 1 to 4. The tether resistance is neglected [8][9][10][11][22] in the simulations made here.

Table 1. Parameters of the Sub-satellites

Dimensions (a_1, a_2)	100 m^2,10 m^2
Mass (m_1,m_2)	1000 kg, 10 kg
C_D	2

Table 2. Parameters of the Tether

Tether core material	Aluminum (2219-T851)
Core density (kg/m^3)	2850
Core resistivity (Ohm*m)	$27.4x10^{-9}$
Tether radius (mm)	0.2

Table 3. Parameters of the Electron Density n_e (e^-/m^3)

Illuminated Area	2.0×10^{12}
Penumbra Area	1.0×10^{11}
Umbra	0.1×10^{11}

Table 4. Nominal Parameters for the Simulations

Nominal semi-major axis (km)	6978 (600 km of altitude)
Eccentricity, Inclination, Argument of Perigee, Eccentric Anomaly, Right ascension of the ascending node	0
Tether length (km)	5
Initial Time	01/01/2014 12:30 GMT

3.2. Introduction of the Tethers

Now it is presented how the electromagnetic tether works for one orbital period of the spacecraft. The analysis is performed by keeping the satellite in a Keplerian orbit all the time. It is also assumed that a thrust is applied to compensate the disturbing forces that the tether cannot reduce.

Figure 1 shows the acceleration considering only the atmospheric drag disturbing force and on the Y axis of the OXYZ reference frame. The orbit is circular and Keplerian, therefore, the Y axis is actually the direction of the orbital motion.

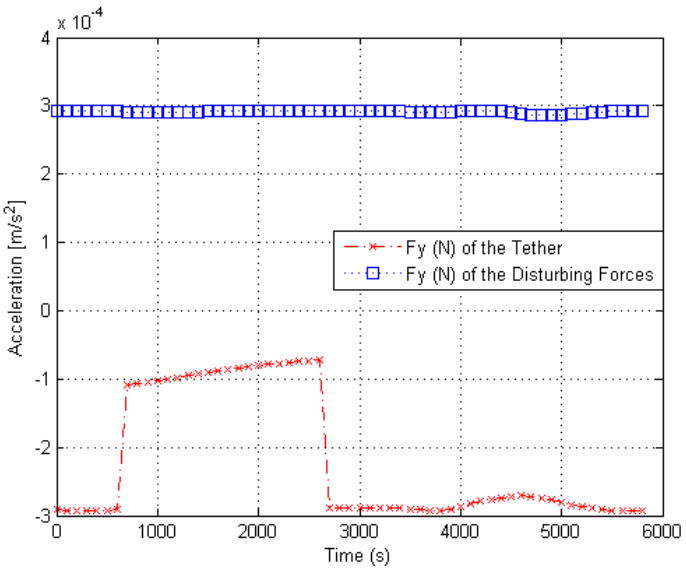

Figure 1. The acceleration of the tether and the atmospheric drag on the Y axis vs. time.

Figure 1 shows that the tether can apply a disturbing force at the opposite direction of the atmospheric drag with almost the same magnitude. There are some intervals where the tether cannot reach the required magnitude. Figure 2 provides the explanation for this limitation.

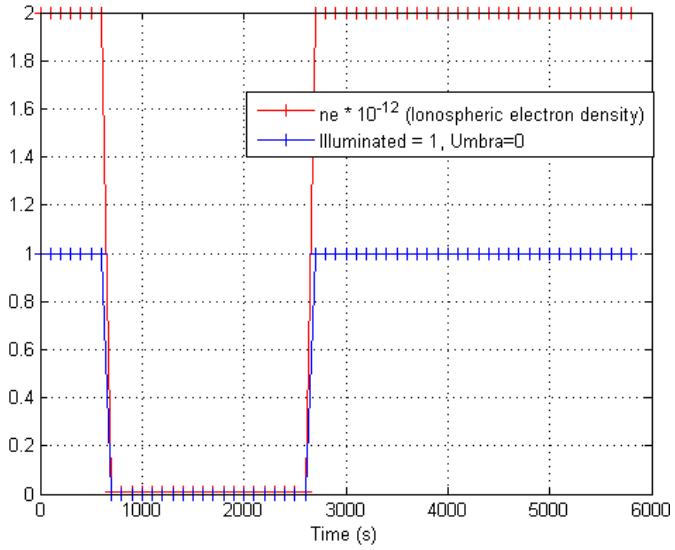

Figure 2. The ionospheric electron density and the illuminated region vs. time.

Figure 2 shows the ionospheric electron density n_e. The n_e is strictly related to the incidence of solar rays. The electron density also defines the current that flows in the tether, as given by Eqs. (2) and (5). The current is related to the magnetic force (Eq. 1) and, if the current is not sufficient to guarantee the optimal magnitude, the tether cannot fully control the disturbing force.

The attitude that the tether must have in this case to reduce the disturbing force of the atmospheric drag is shown in Fig. 3.

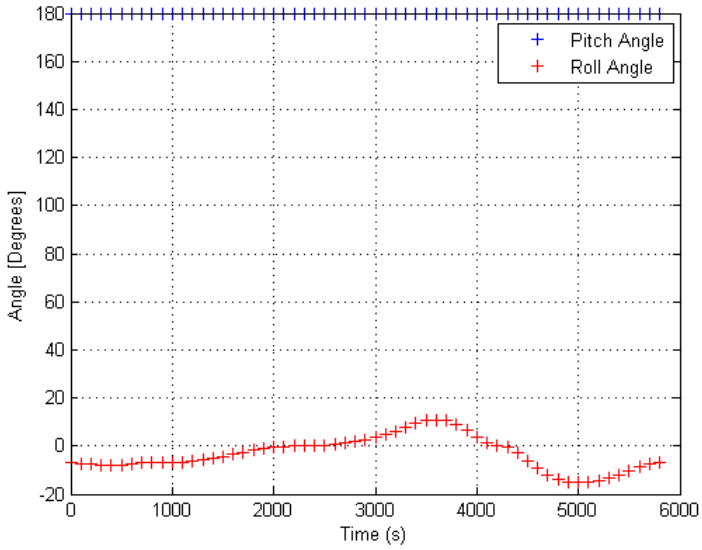

Figure 3. Pitch and the Roll angles vs. time.

The pitch angle remains steady all the time, at 180 degrees. The 180 degrees means that the direction of the tether remains parallel to the position vector, as expected. The current flow requires a battery to drive the current into the opposite direction of the induced EMF, therefore the pitch angle is 180 degrees. In the case of a de-orbit, the tether would be required to act as a drag, so the pitch angle should be zero. The roll angle is not zero. The attitude direction of the tether is based on the centre of mass of the system. At that point, the roll is optimal and guarantees that the direction of the electromagnetic tether force along with the pitch angle is opposite to the direction of the disturbing forces. The power and the current that the tether must provide in order to perform this maneuver is shown in Fig. 4.

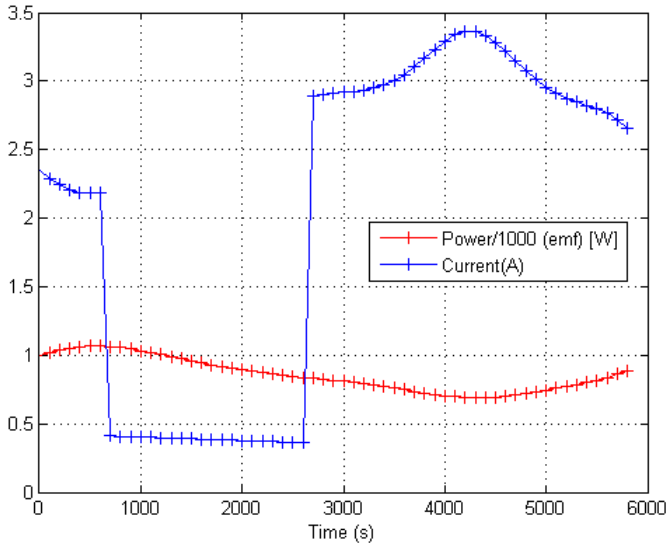

Figure 4. Current and power vs. time

The power shown in Fig. 4 is the power that the battery must apply in order to guarantee that the current flows in the right direction. The current is the one that must flow in the tether to guarantee that the magnitude of the tether force is coherent with the magnitude of the disturbing

force. The current shown in Fig. 4 is not the maximum value that the tether can deliver to the system (see Eq. (5) for the maximum current definition). For this simulation, the maximum current is around 20 A. This means that the tether itself can also allow a current flow larger than the one shown in Figure 4 to overcome the gap of the current through the passage by the umbra region.

The PI integral, without the averaging technique ($inte$), as given by Eq. (10), can provide the amount of the magnitude reduction of the disturbing force for this maneuver. Table 5 provides the $inte$ values for the tether and for the disturbing force.

Table 5. $inte$ **values based on Eq. 10**

Atmospheric Drag	1.7127 m/s
Tether only	1.2173 m/s
Atmospheric Drag + Tether	0.6299 m/s

Table 5 shows the efficiency of the tether proposed in this context. The atmospheric drag has the $inte$ value of 1.7127 m/s. This means that the velocity delivered to the spacecraft due to this disturbing force for one orbital period is 1.7127 m/s. It would be required a thrust with a total velocity change of this magnitude for one orbital period to guarantee that the satellite does not deviates from its orbit. The tether itself delivers a $inte$ value of 1.2173 m/s to the system. The combination of the atmospheric drag and the tether has a $inte$ value of 0.6299 m/s. The optimal direction of the tether requires a long processing time for the computer. The method of defining the attitude of the tether based on the centre of mass of the system is fast, but it involves also some errors due to the asymmetry of the magnetic field and its fluctuations. The price of not computing the fluctuations on the magnetic field of the Earth is that the subtraction of the $inte$ value of the atmospheric drag and the tether itself is not the $inte$ value of the atmospheric drag and the tether.

The tether proposed in this work for this specific maneuver could reduce the magnitude of the disturbing force of the atmospheric drag up to 63.22 %. The tether has 5 km length, which is enough for the proposed mission. The current necessary to reduce the magnitude of the disturbing force ($\approx 3\ A$) is far lower from the maximum value ($\approx 20\ A$).

The next step is to study the case where the tether will not only reduce the atmospheric drag, but also the other disturbing forces: third-body perturbation of the Sun and the Moon and the solar radiation pressure. Figures 5 and 6 show the acceleration of the tether and the sum of all disturbing forces as a function of time. The component of the Z axis was omitted, because the magnitude of the disturbing force on this axis is much smaller compared to the other two components.

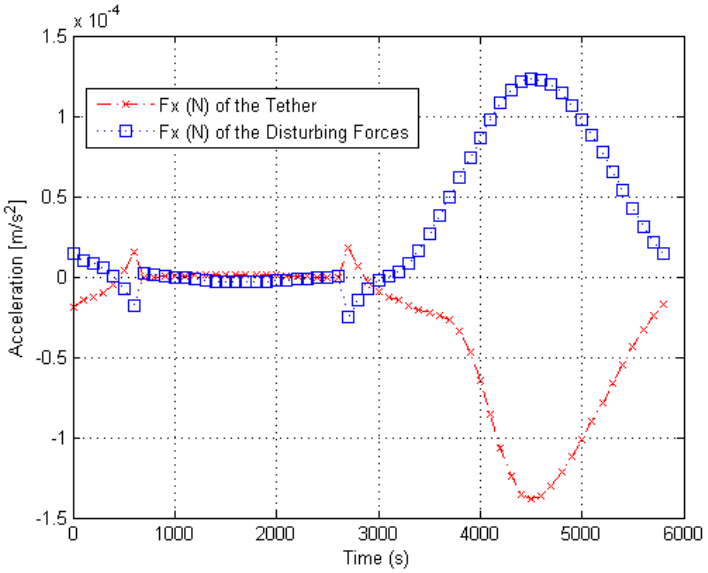

Figure 5. Acceleration of the tether and all the perturbations on the X axis vs. time.

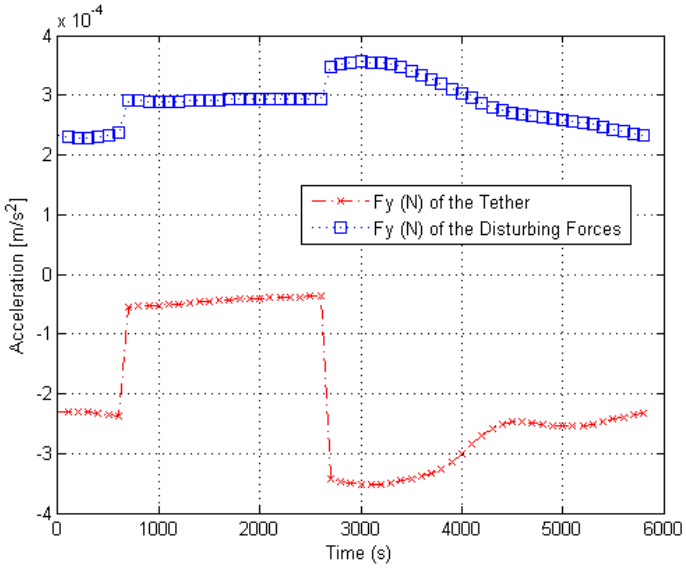

Figure 6. Acceleration of the tether and all the perturbations on the Y axis vs. time.

It is clear that the accelerations of the tether and the disturbing forces are almost opposite. Since the initial time of the simulation and the initial parameters are the same, it is possible to note that there is the same gap of the acceleration of the tether for an interval of the time. This occurs, as shown in Figure 2, due to the passage of the spacecraft by the shadow of the Earth. It is also interesting to note that the acceleration of the disturbing forces shown in Figs. 5 and 6 also has a discontinuity. The passage by the shadow area reduces the solar radiation pressure perturbation to zero and, therefore, there is a decrease in the sum of all perturbation for this interval as well.

The attitude of the tether, given by the pitch and the roll angles, is different from the previous maneuver. Now the sum of all the disturbing forces changes the direction that the tether

force must be applied. Figure 7 shows the pitch angle that the tether must have for this maneuver. The roll was neglected, since it does not play an import role in this simulation.

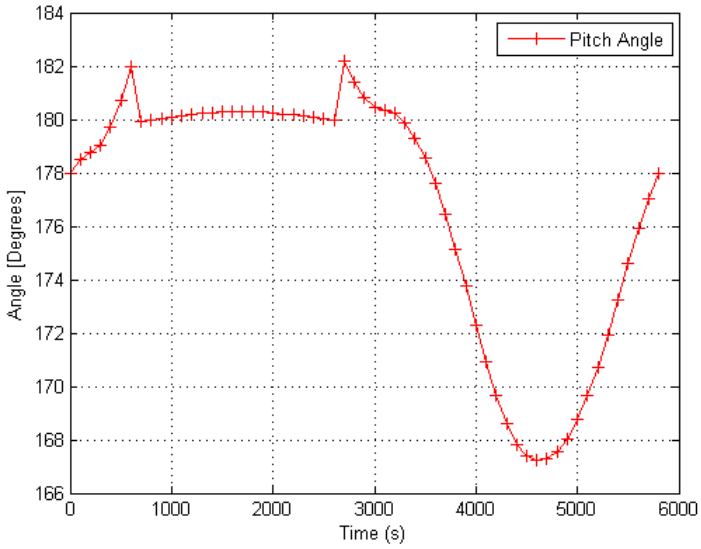

Figure 7. Pitch angle vs. time.

There is a discontinuity of the pitch angle due to the decrease of the solar radiation pressure perturbation at the shadow region. Besides this discontinuity, the change of the pitch angle is smooth and changes from 180 to 167 degrees. If it is possible to build a tether that can change and control of the pitch angle, then it is possible to reduce all disturbing forces included in this paper. The advantage of reducing all the disturbing forces is to reduce the secular and periodic variations. The PI reduction with this maneuver is given in Table 6. The reduction of the magnitude of the disturbing forces is 62.46 %.

Table 6. *inte* value based on Eq. 10

All perturbations	1.7177 m/s
Tether only	1.2223m/s
All perturbations + Tether	0.6449 m/s

3.3 The Perturbation Integrals Results

This section shows the PI obtained using the averaging technique. The PI is the *inte* integral with an averaging technique that provides the mean value of the *inte* for one year. This method evaluates in a fast and easy way the potential that the tether has to reduce the magnitude of the disturbing forces.

The initial parameters are given in section 3.1. The first result, shown in Fig. 8, changes the semi-major axis of the orbit from 6678 to 6978 km (300 to 600 km of altitude). The integration of one orbital period is multiplied by the period of a nominal reference orbit and divided by the period of the current orbit, to avoid a time dependence of the results. The nominal reference orbit is given in Table 1 (6978 km of semi-major axis). Figure 8 shows the PI when the tether is used only to reduce the atmospheric drag.

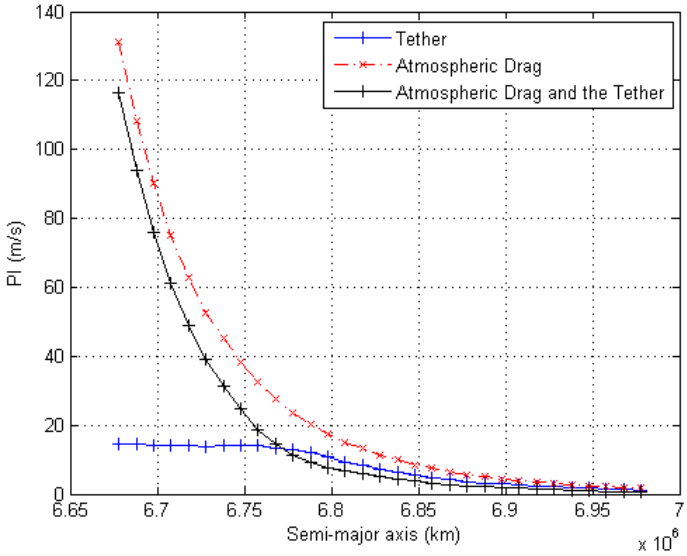

Figure 8. PI vs. Semi-major axis.

Figure 8 shows that the tether is efficient in reducing the magnitude of the disturbing forces. This reduction could be better, if different tether lengths are considered for each semi-major axis interval. The reduction of the magnitude close to the 6678 km of semi-major axis is low, due to the magnitude of the atmospheric drag. The magnitude is so large that, even using the maximum current I_{max}, the tether is not able to guarantee that the disturbing forces can have the same magnitude (see Fig 9).

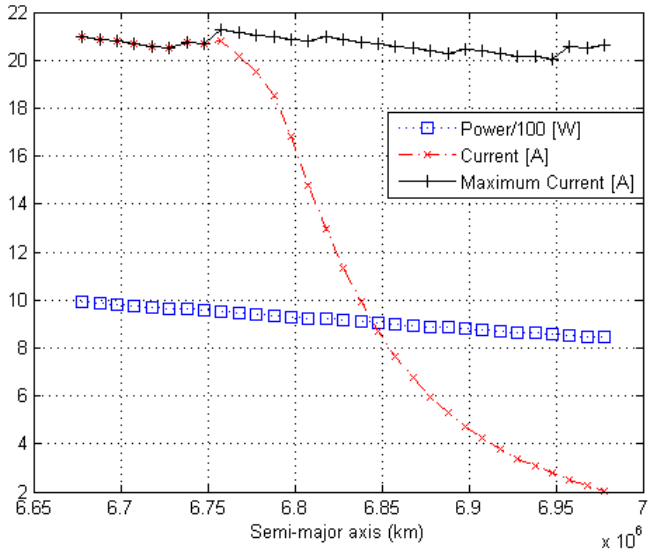

Figure 9. Current and Power of the Tether vs. Semi-major axis.

Figure 9 shows the maximum current and the nominal current to reduce the disturbing forces. From 6678 to 6750 km of semi-major axis, the nominal current of the tether is the maximum value. Therefore, for this case, the magnitude of the tether cannot be the magnitude of the disturbing force due to the current restriction of the bare tether.

Figures 10 and 11 show the use of the tether to reduce all the disturbing forces that this paper considers. The range of the semi-major axis goes from 6978 to 7278 km.

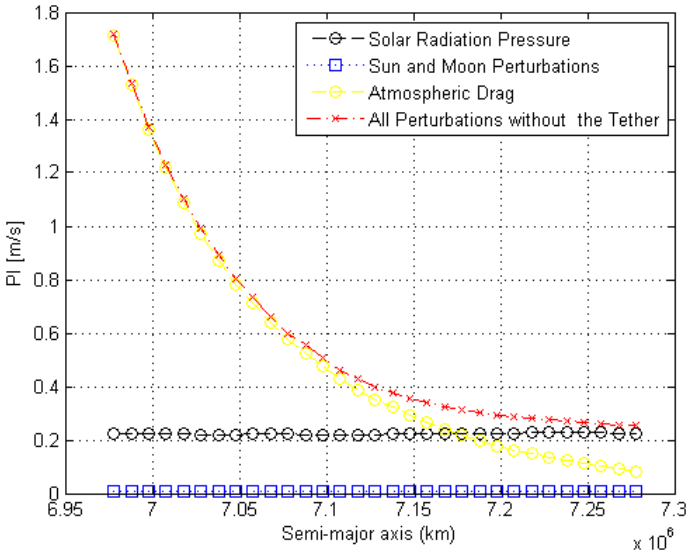

Figure 10. PI vs. Semi-major axis.

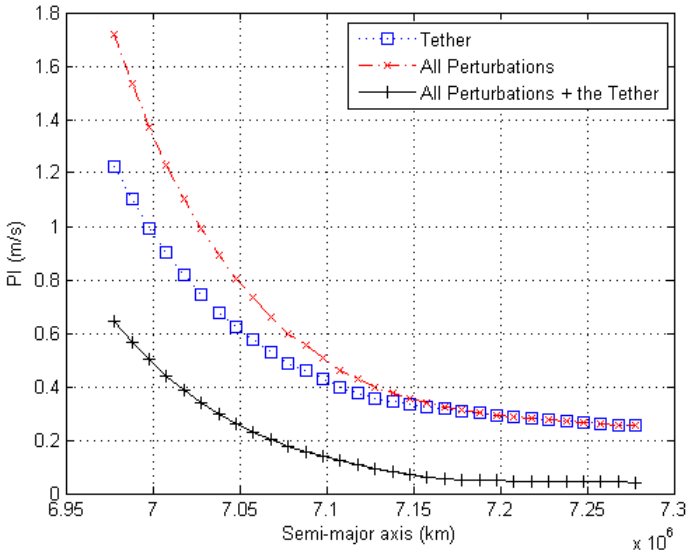

Figure 11. PI vs. Semi-major axis.

The tether can reduce better the disturbing forces when the semi-major axis increases, because there are fewer passages by the umbra region, so the spacecraft has more electron density to reduce the disturbing forces.

The next simulation shows the study of the PI as a function of the inclination of the orbit. As the inclination of the orbit increases, the induced EMF decreases. The power used to drive a current on the opposite direction of the induced EMF decreases. Figure 12 shows a simulation with the initial parameters given in section 3.1, except for the orbit inclination, which in this case varies from 0 to 90 degrees.

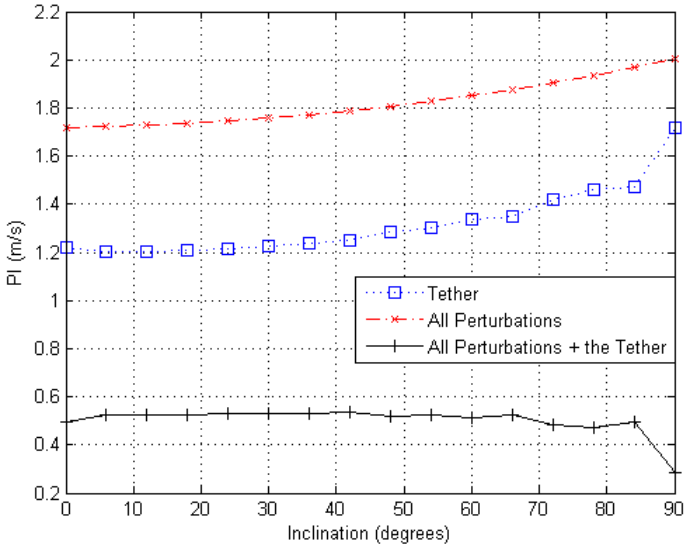

Figure 12. PI vs. Inclination of the Orbit.

The magnitude of the force due to the tether increases as the inclination increases. The induced EMF decreases when the inclination of the orbit increases. Therefore, there is less power that the battery must provide to overcome the EMF. Nevertheless, although the tether works as an efficient way to reduce the disturbing forces, the roll attitude at the orbital inclination of 90 degrees varies from 0 to 90 and from 270 to 360 degrees along one orbital period and the pitch angles varies from 0 to 360 degrees. This occurs due to the geometry of the magnetic field. Although it seems promising the application of this method for highly inclined orbits, the pitch angle variation demands more challenges from the attitude control. Figure 13 shows the pitch and roll angles for the simulation with 90 degrees of inclination.

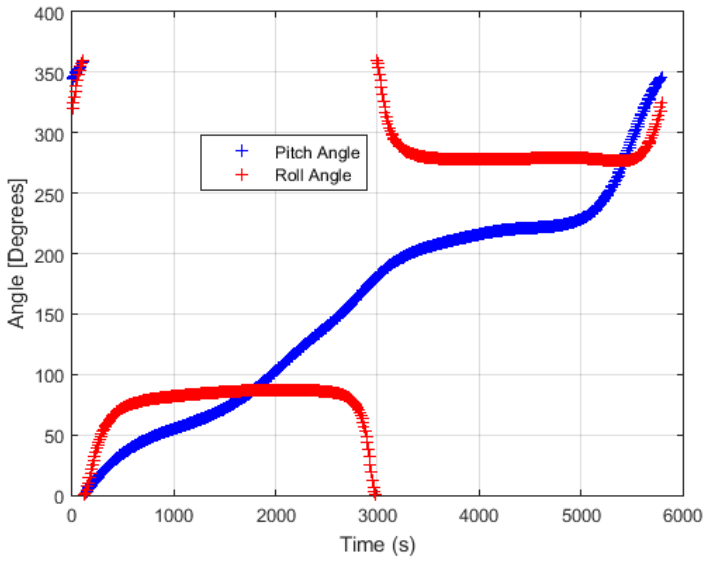

Figure 13. Pitch and Roll angles vs. time.

The pitch angle varies from 0 to 360 degrees. It means that the direction of the current changes. This change occurs with the signal change of the EMF as well. This means that, even if

the current changes the direction, the battery still has to provide power to overcome the EMF. In this case, it is assumed that the current can flow in both directions of the tether and that both end masses can emit electrons. The drastically change of the pitch angle is related to the direction of the magnetic field at the poles of the Earth. At the poles, the direction of the magnetic field becomes radial and this fact results in a change of the tether direction from mainly radial to the direction of the orbital velocity, to guarantee that the tether can reduce the disturbing forces, mainly the atmospheric drag. Figure 14 shows the power that the battery must provide or the induce EMF and the current to perform the maneuver for different orbital inclinations.

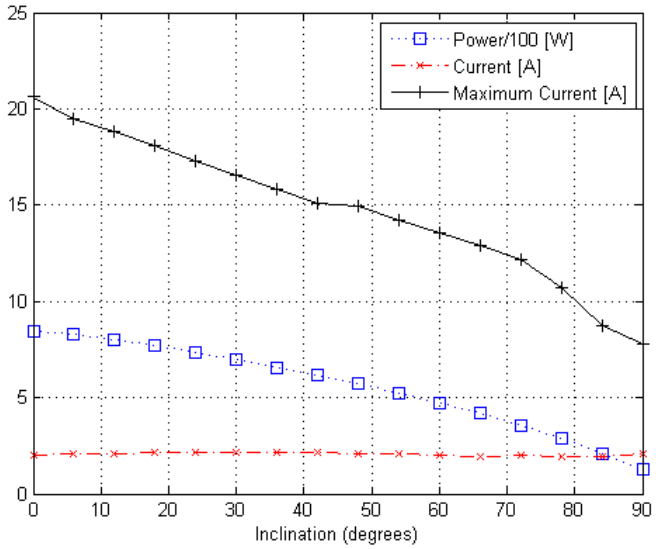

Figure 14. Current and Power of the Tether vs. Inclination.

The current required for the station-keeping maneuver is almost constant, although the power required from the battery decreases as the inclination increases. The maximum current decreases, as well as inverse EMF and the motional electric field decreases (see Eqs. (2), (3) and (5)).

3.3 The Orbital Propagator Results

This section simulates the spacecraft trajectory with an orbit integrator. The initial parameters of the simulation are given in section 3.1. Figure 15 shows three trajectories: i) considering only the external perturbations (no tether), ii) considering the external perturbations and the tether to reduce only the atmospheric drag; iii) considering the external perturbations and the tether to reduce all the perturbations. The integration is performed for 13.5 days (20 orbital periods of the nominal orbit).

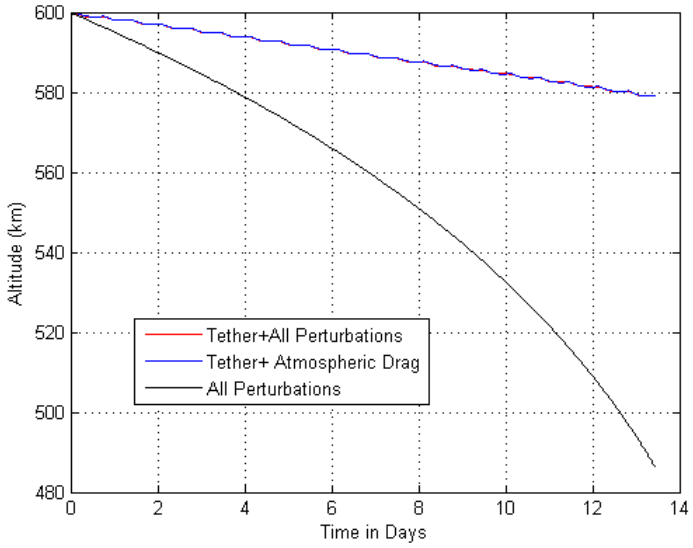

Figure 15. Altitude vs. Time in days.

It is clear that the tether reduces the deviations caused by the atmospheric drag. The decay of the orbit using the tether is much smaller for the same integration time. The situation where the tether is used to control the atmospheric drag and all the disturbing forces provides almost the same results. This occurs because the atmospheric drag is the main perturbing force in this trajectory.

4. Conclusion

The main objective of this paper is to study how much an electromagnetic tethers can help in reducing the external disturbing forces received by a spacecraft in the orbit of the Earth. The idea behind this paper is very powerful for future missions, when this technology can be used. When the spacecraft achieves the end of its mission, the electromagnetic tether can also be used to de-orbit the spacecraft to eliminate this large potential space debris.

The results show that the tether can reduce a large portion of the disturbing forces. Nevertheless, the efficiency of the tether depends on the sunlight. The passage by the umbra or the penumbra in part of the trajectory reduces the efficiency of the tether.

A first analysis of the potential that the tether has to reduce not only the atmospheric drag and re-boost the orbit, but also to reduce others disturbing forces, is extremely positive.

The idea of reducing the perturbations at every step of time has some advantages, if compared to re-boosting rapidly the spacecraft with the tether. The method proposed here provides low currents as the magnitude of the disturbing forces are reduced at every step. The control attitude deals with less internal torques and with lower currents flowing through the tether.

5. References

[1] Hacker, B. C., Alexander, C. C., “On the Shoulders of Titans: A history of Project Gemini”, NASA Special Publication, 4203 in the NASA History Series, 1977, pp. 361, 366-368, 378,379.

[2] Jablonski, A. M., Vigneron, F. R., Tyc, G., Han, R. P. S., Misra, A. K., Modi, V. J., Chandrashaker, R., "OEDIPUS-C Tether Dynamics Experiment", 9th CASI Conference on Astronautics, Ottawa, ON, Nov. 13-15,1996.

[3] Cosmo, M. L., and Lorenzini, E.C., "Tethers in Space Handbook", 3rd Edition, Smithsonian Astrophysical Observatory, Cambridge, MA, 1997.

[4] Forward, R. L., Hoyt, R. P., Uphoff, C., "The Terminator Tether: A Low-Mass System for End of Life Deorbit of LEO Spacecraft", Tether Technical Interchange Meeting, Huntsville, AL, Sept 10 1997.

[5] Purdy, W., Coffey, S., Barnds, W. J., Kelm, B., Dabis, M., "TiPS: Results of a Tethered Satellite Experiment", presented at the AAS/AIAA Astrodynamics Specialist Conference, Sun Valley ID, Aug. 4-7 1997, Paper No. AAS-97-600.

[6] Lanoix, E. L. M., "A mathematical model for long-term dynamics of tethered spacecraft", Thesis of the Department of Mechanical Engineering, McGill University, Montreal, June 1999.

[7] Alpatov, A. P., Beletsky, V. V., Dranovskii, V. I., Khoroshilov, V. S., Pirozhenko, A. V., Troger, H., Zakrzhevskii, A. E., "Dynamics of Tethered Space Systems", ISBN 978-1-4398-3685-9, 2010.

[8] Johnson, L., Herrmann, M., "International Space Station – Electrodynamic Tether Reboost", Marshall Space Flight Center, Marshall Space Flight Center, Alabama, NASA/TM-1998-208538.

[9] Estes, R. D., Sanmartin, J.R., and Martinez-Sanchez, M., Technology of Bare Tether Current Collections, Tether Technology Interchange Meeting, Nasa Marshall Space Flight Center, Hunstville, AL, Sept.9-10,1997.

[10] Lorenzini, E.C., Estes, R. D., and Cosmo, M.L.,"Electrodynamic Tethers for the International Space Station", In-Space Transportation with Tethers, Annual Report for NASA GRANT NAG9-1303, Smithsonian Astrophysical Observatory, Cambridge, MA, Oct. 1997.

[11] Lanoix, E.L.-M. and Misra, A.K., Modi, V.J. and Tyc, G., "Effect of electromagnetic forces on the orbital dynamics of tethered satellites", AAS/AIAA Space Flight Mechanics Meeting, Clearwater, FL, January 2000, Paper No. AAS-00-189.

[12] Steiger, C., Romanazzo, M., Emannuelli, P.P., "Drag-free Attitude and Orbit Control System Performance of ESA'S GOCE Mission during Low Orbit Operations and De-orbiting", SpaceOps Conferences, 5-9 May 2014, Pasadena, CA, AIAA 2014-1906, DOI: 10.2514.6.2014-1906

[13] Canuto, E., Massotti, L., Molano-Jimenez, A., Perez, C.N., "Drag-free and attitude control for long-distance, low-Earth-orbit, gravimetric satellite formation", Control Conference (CCC), 2010 29th Chinese, 29-31 July 2010, p. 5408 – 5413, IEEE publisher, ISBN 978-1-4244-6263-6

[14] Canuto, E., Colangelo, L., Buonocore, M., Massotti, L., Girouart, B., "Orbit and formation control for low-earth orbit gravimetry drag-free satellites", Proceedings of the Institution of Mechanical Engineers, Part G: Journal of Aerospace Engineering June 2015 vol. 229 no. 7 1194-1213, September 21, 2014, doi:10.1177/0954410014548236

[15] Lange, B., "The Drag-free Satellite", AIAA Journal, Vol.2 NO. 9, p. 1590-1606

[16] Prado, A. F. B. A., "Searching for Orbits with the Minimum Fuel Consumption for Station-Keeping Maneuvers: Application to Luni-Solar Perturbations." Mathematical Problems in Engineering (Print), Volume 2013(2013), Article ID 415015, 11 pages.

[17] Oliveira, T. C., Prado, A. F. B. A., "Mapping orbits with low station keeping costs for constellations of satellites based on the integral over the time of the perturbing forces", Acta Astronautica, Volume 104, Issue 1, Pages 350-361, November 2014.

[18] Davis, J., "Mathematical Modeling of Earth's Magnetic Field", Technical Note, Virginia Tech, Blacksburg, VA 24061, May 12, 2004

[19] Wertz, J. R., (1978), "Spacecraft Attitude Determination and Control", London, D. Reidel.

[20] Iyemori. Website about International Geomagnetic Reference Field (IGRF-11), online: http://wdc.kugi.kyoto-u.ac.jp/igrf/index.html

[21] IAGA Division V-MOD Geomagnetic Field Modeling. International Geomagnetic Reference Field, online: http://www.ngdc.noaa.gov/IAGA/vmod/igrf.html

[22] Sanmartin, J. R., Martinez-Sanches, M., Ahedo, E., "Bare Wire Anodes for Electrodynamic Tethers", Journal of Propulsion and Power, Vol. 9, 1993, pp.353-360.

[23] Tewari, A., "Atmospheric and Space Flight Dynamics", Birkhauser, ISBN -10:0-8176-4373-7.

[24] Committee on Extension to the Standard Atmosphere (COESA): U.S. Standard Atmosphere 1972. U.S. Government Printing Office, Washington, DC (1976).

[25] COESA: U.S. Standard Atmosphere 1962. U.S. Government Printing Office Washington, DC (1962).

[26] Capó-Lugo, P. A., Bainum, P. M., "Orbital Mechanics and Formation Flying – A digital control approach", ISBN: 978-0-85709-054-6.

[27] Fieseler, P. D., "A Method for Solar Sailing in a Low Earth Orbit", Acta Astronautica Vol. 43, No. 9-10, pp.531-541,199.